TITLE: Establishing the Macular Grading Grid by Means of Fovea Centre Detection Using Anatomical-Based and Visual-Based Features

AUTHOR:

Arturo Aquino

Email: arturo.aquino@diesia.uhu.es

Tlfn: (+34) 959217590

Department of Electronic, Computer Science and Automatic Engineering,

"La Rábida" High School of Engineering,

University of Huelva,

21819 Palos de la Frontera,

Spain

ABSTRACT

This paper presents a methodology for establishing the macular grading grid in digital retinal images by means of fovea centre detection. Usually, visual and anatomical feature based criteria have been used separately for fovea segmentation. However, the combination of the benefits of both techniques constitutes the core methodology presented throughout this paper. Firstly, an acceptable fovea centre estimation is obtained by using a priori-known anatomical feature with respect to the optic disc and the vascular tree. Secondly, a type of morphological processing attempts to improve the obtained fovea centre estimation when the fovea is detectable in the image; otherwise it is declared indistinguishable and the first result is retained. The methodology was tested on the MESSIDOR and DIARETDB database using a distance criterion between the obtained and the real fovea centre. Fovea centres in the brackets between Excellent-Fair (fovea centres primarily accepted as valid in the literature) made up 97.42% and 95.51% of all cases in the MESSIDOR and DIARETDB, respectively.

INDEX TERMS: retinal diseases, early diagnosis, retinal imaging, macular grading grid establishing, fovea segmentation.

I. INTRODUCTION

Diabetic retinopathy (DR) is a retinal disease, derived from complications caused by diabetes mellitus, which is the leading cause of blindness among people of working age in developed countries [1]. The estimated prevalence of diabetes for all age groups worldwide is forecasted to rise from 171 million in 2000 to 366 million in 2030 [2]. Although DR is not a curable disease, laser photocoagulation can prevent major vision loss if the illness is detected in early stages [1], [3]. However, diabetic patients unfortunately do not undergo DR symptoms until visual loss develops, usually in its later stages, when treatment is less effective. In effect, to ensure that treatment is received in time, diabetic patients are examined annually by their public health systems [4]–[6]. Within this context and due to the huge number of patients needing this periodical revision, the use of computer-aided DR diagnosis by means of digital retinal image analysis can improve the effectiveness of the early detection of the illness.

The macula plays a key role in assessing DR and other ophthalmic pathology conditions, such as age-related macular degeneration or macular edema. Since the macular zone is responsible for sharp central vision, the location of lesions with respect to this influences their clinical relevance. Therefore, successful identification of the macula is of vital importance for the development of systems for the automated diagnosis of DR and other diseases.

This paper proposes a new highly reliable methodology for detecting the macula centre and ultimately establishing the macular grading grid. To detect the macula centre, previous works have usually employed one of the following approaches: segmentation of the macula centre, or macula centre estimation by means of its a-priori known positional features on the retinal surface. Using the first approach, the macula centre can be obtained more accurately than using the second one. However, since the macula centre is not occasionally visible (discussed later), the second approach is more reliable. For these reasons, the methodology proposed in this paper attempts to exploit and combine the benefits of both approaches. The methodology proposes to obtain an acceptable macula centre location estimation for all cases, and the replacement of this first result with an accurate location when it is safe and possible; this is, when the macula centre is visible.

The rest of the paper is structured as follows: characterization of the macula can be found in Section II. Section III reviews the state of art of methods for automated macula centre detection. Section IV defines the material used in this work. The new methodology is described In Section V, whereas Section VI presents the obtained results. Finally, this paper concludes with the author's discussion and conclusion.

II. MACULA CHARACTERIZATION

The macula is a round area in the central region of the retina, which measures about 3 to 4 mm in diameter. As commented before, the macula provides the most distinct vision and is responsible for central vision. There is a small depression in the centre of the macula measuring about 1 mm in diameter and visible as a round dark area called the fovea. The whole macula is not generally distinguishable in retinal colour images. It exhibits non-specific structure and varies greatly across individuals due to variations in the levels of pigment associated to factors such as ethnicity, age, diet, and disease condition. In spite of this, the fovea is often recognizable as a round region darker than its surrounding retinal tissue (Figure 1 - (a)). However, this mark may not be visible due to, for example, the presence of lesions (Figure 1 - (b)). Anatomically, the fovea centre is located at 2.5 optic disc (OD) diameters in average from the OD centre [7]. The fovea location follows the horizontal raphe of the retina, which is a line roughly passing through the OD and the fovea, or more generally, separating the superior and inferior regions of the retina determined by the superior and inferior vessels of the vascular tree. This raphe is rotated a few degrees with respect to an imaginary horizontal raster passing through the OD centre. The fovea radius is between one third and one fourth of the macula radius, and the macula radius is approximately equal to one OD diameter [8] (Figure 2).

III. STATE OF ART

According to literature, two types of criteria for macula segmentation can be clearly recognized. These can be identified as visual and anatomical feature-based criteria. The former criterion includes techniques that attempt to find the macula by exploiting the visual appearance of the fovea. On the other hand, the latter criterion comprises techniques to obtain an estimation of the fovea centre location making use of its known anatomical features regarding its position on the retinal surface.

Sinthanayothin et al. [15] presented a methodology for fovea recognition in which it was assumed to be the darkest area of the fundus image. Firstly, they correlated the fovea to a template of intensities. Then, the location of the maximum response was selected as the location of the fovea if it was at approximately 2.5 times the diameter of the OD from the OD centre. Gagnon et al. [12] used a similar approach to detect the macula centre. They generated a coarse resolution image in which they selected the darkest pixel. Then, by searching its vicinity for the darkest pixel on the original image, the exact macula centre was found. On the other hand, Li and Chutatape [13] combined this approach with the use of the vascular arch to constrain the search area. As a result, they presented a model-based approach in which an active shape model was used to extract the main course of the vasculature based on the location of the OD. This course and the distance criterion of the fovea were used to decide on an area of interest. Finally, the fovea centre was obtained by applying a thresholding scheme to the region of interest. Tobin et al. [10] proposed the automatic location of the fovea using the distance criterion and the vascular arch exclusively. The method started by locating the OD and estimating the vascular arch by using a parabolic model. Based on these two anatomical landmarks, the location of the fovea was ultimately inferred. A similar method for fovea recognition was presented by Fleming et al. [11]. The method found the locations of the OD and the fovea by modeling the major retinal blood vessels. Finally, the position of the fovea was refined based on its local darkening. On the other hand, Niemeijer et al. [9] presented a method to model the distribution of all retinal features. The method used an optimization method to fit a point distribution model to the fundus image. After fitting, the points of the model indicated the location of the normal anatomy.

These same authors later presented another work on the detection of the fovea [14]. They first found the OD and, based on its location, determined an area of interest for the fovea. Then, after blurring the image, its location was decided as the pixel with the lowest value within the restricted area. Welfer et al. [16] proposed the fovea centre detection by making use of anatomical knowledge and mathematical morphology. They firstly calculated the centre and diameter of the OD with the aim of extracting a fovea-containing region of interest. Then, they applied a morphological processing with which they obtained a set of fovea candidates. Finally, they selected as the fovea centre the centroid of the darkest candidate located below an imaginary horizontal line passing through the OD centre. Narasimha-Iyer [17] et al. presented a two-step approach method for locating the fovea centre. Making use of the known distance between the OD and the fovea, they extracted a region on interest and applied an adaptive threshold to segment the target. A visual-feature based methodology was proposed by Singh et al. [18]. Essentially, they performed a local contrast enhancement and found a dark structure which was identified as the fovea. Sagar et al. [19] combined visual and anatomical features to decide on the fovea centre. Firstly, they detected a region of interest in the image using the distance rule between the OD and the fovea. Then they masked out all blood vessels pixels in this subimage using morphological operations. Afterwards, the darkest pixels were identified and clustered. The centroid of the largest cluster was selected as the fovea centre. Sopharak et al. [20] used a similar approach to find the fovea. In their first step, they estimated the fovea position by using the OD diameter, and then they masked out the high contrast vessels using morphological processing. On the other hand, Sekhar et al. [21] proposed the use of morphological processing and thresholding to detect the fovea. Primarily, they calculated the OD centre and boundary using morphological processing and the Hough Transform. Then, using the spatial relationship between the OD diameter and the fovea region they extracted a region of interest. Finally, the fovea centre was obtained by applying thresholding and morphological operators.

IV. MATERIAL

For development and testing of the work presented here the MESSIDOR and DIARETDB database were used.

The MESSIDOR database [22], kindly provided by the MESSIDOR program partners, contains 1200 RGB eye fundus colour images of the posterior pole acquired by the Hôpital Lariboisière Paris, the Faculté de Médecine St. Etienne and the LaTIM - CHU de Brest (France). 800 of these images were captured with pupil dilation (one drop of Tropicamide at 10%) and 400 without dilation, using a Topcon TRC NW6 non-mydriatic retinograph with a 45º FOV. The images are 1440 x 960, 2240 x 1488 or 2304 x 1536 pixels in size, 8 bits per colour plane and are provided in TIFF format. DR and risk of macular edema diagnoses were provided by medical experts for each image. 540 correspond to healthy patients and 600 images are from patients affected by DR with or without risk of ME.

On the other hand, the DIARETDB database [23] is composed of 89 RGB colour retinal images of which 84 show DR affection. The images were taken in the Kuopio university hospital and selected by medical experts. Database's partners inform that the dataset is biased, so the distribution of cases does not correspond to any "natural" cases distribution. Images were captured using a 50º field-of-view and are 1500x1152 pixels in size.

V. METHODOLOGY

This paper describes a new methodology to establish the macular grading grid in retinal images by means of fovea centre detection. Since the fovea is not always visible and the main objective is to obtain a good result for all cases, the methodology proposed here make use of both visual and anatomical feature-based criteria. The way in which the benefits of both approaches are exploited distinguishes this work from others previously published. Respectively, the philosophy of the methodology is primarily to obtain a provisional result based on an acceptable estimation of the macula centre using its known positional features with respect to the OD and vascular tree. Thus, once the estimate is acquired it is then replaced with an accurate macular centre location by means of

the fovea segmentation when visible; if the fovea is not detectable then the first result is not replaced. The methodology is divided into three main stages: A) obtaining a macula centre location estimation, B) obtaining an accurate fovea centre location, and C) final decision of the macula centre location and macular grading grid establishing.

A. Obtaining a Macula Centre Location Estimation

The primary approach for estimating the macula centre is to determine the horizontal raphe of the retina, or in other words, the line delimiting the superior and inferior vessels. The fovea centre is assumed to reside at a fixed distance along this line at 2.5 OD diameters from the OD centre [7]. Therefore, to obtain the retinal raphe estimation and ultimately estimate the fovea location, the segmentations of the OD and vascular tree are required. The methodologies presented in [24] and [25] for the segmentation of these landmarks are used all throughout this work. D_{OD} and (x_{OD}, y_{OD}) will denote the diameter and the coordinates of the OD centre, respectively, and $b_t\ (x, y)$ will stand for the segmentation of the vasculature structure skeletonized using an homotopic skeletonization method [26] (see Figure 3, images (a) and (b)).

To estimate the horizontal raphe of the retina, a parabolic model with origin in (x_{OD}, y_{OD}) is applied to $b_t\ (x, y)$. Thus, the angle between the horizontal raster and the line of symmetry separating the superior and inferior retinal regions is identified (see illustration in Figure 3). In essence, the model proposed by Tobin et al. in [10] is used.

Once the raphe of the retina is obtained, most of works present in the literature estimate that the fovea centre is at 2.5 * D_{OD} pixels from (x_{OD}, y_{OD}) following the raphe. Generally, this measurement is valid, however, certain cases were identified in our dataset of 1200 images of which this rule was not accomplished due to their abnormally large and small OD sizes. Indeed, this is a consequence of 2.5 * D_{OD} pixels is an average distance, since it is known that the OD size varies substantially from one tenth to one fifth of the retina [27]. To solve this difficulty, a criterion to detect and discard D_{OD} values in the extremes of the interval of OD size values was introduced. To define this criterion, firstly the maximum OD diameter was measured in each gold standard of the MESSIDOR OD gold standard set available at [28]. Then, the ratios between these OD diameters and

the diameters of their corresponding field-of-view masks (FOVs) were calculated. Thus, the distribution of the relative OD size measured in the whole set independently of image resolution was obtained. The distribution of these calculated ratios normalized to the interval [0, 1] is presented in Figure 4. As it can be seen, the figure shows that normalized ratios follow a Gaussian distribution, whose average and standard deviation are 0.1382 and 0.0149, respectively (note that the obtained distribution corroborates that OD size is between one tenth and one fifth of the retina). Therefore, the criterion to discard a D_{OD} value is to consider this as extreme if its value is out of the average of the distribution plus/minus 2 times the standard deviation (i.e., out of the 95% of the distribution approximately). In this case, the discarded OD diameter value is replaced by the average value of the normal distribution.

Figure 5 shows some examples of the application of the described methodology for estimating the fovea centre. The first row shows results on images from patients affected by DR with no risk of ME, the images in the second row are from patients affected by DR with risk of ME and the last row shows results on images from healthy patients. Drawn on the images is the parabolic fit to the vasculature. The drawings on the images also include the position of the located OD centre, the segmented OD boundary and the placement of the estimated macula centre along the raphe.

B. Obtaining an accurate fovea centre location

The aim of this stage is to attempt to find an accurate fovea centre location by taking advantage of the estimation obtained in the previous step. Since the fovea is not always discernible, the main idea is to detect if a dark object exists in the image, having a certain depth, and decide on, according to its shape and size whether it matches with a typical fovea. If this object exists and is validated, a new accurate fovea centre location is decided as the centroid of this object. Otherwise, the fovea is considered undetectable and the result of the present stage is null.

The processing described in this section works on an RGB subimage which was extracted from the original retinography using the fovea location estimation obtained in the previous stage. Centered on this location, a $2 * D_{OD}$ x $2 * D_{OD}$ fovea-containing subimage is extracted to be processed.

Although it is known that the green channel of an RGB retinography is the one with highest contrast [29], on observing our imagery it was revealed that when the fovea is visible in the colour image it is also often present in the red channel. Therefore, the processing described in this section is performed in parallel on the red and green components and the "better" of the two results is ultimately selected.

1) Obtaining fovea candidates:

The fovea is visible as a round dark region delimited by a soft frontier when this is discernible. This region is usually darker in its centre and gradually brighter as its frontier is reached. Therefore, the fovea can be seen conceptually as a soft valley which is recognizable if it is deep enough.

Let I be the fovea-containing subimage from the red or the green field (Figure 6, images R and G). In order to filtrate from I those minima that are too shallow to be considered the fovea, the H-minima transform [30] is used. This transform suppresses all minima in the image whose depth is less than a scalar h (Figure 6, images R-1 and G-1):

$$I_F = Hmin(I, h) \tag{1}$$

The choice of the value for parameter h is not especially critical. Tests made with our imagery indicate that a good h value is 15, although values slightly higher or lower are also valid and provide almost the same detection results.

Once irrelevant minina in I have been suppressed, surviving regional minima in I_F are segmented. In order to perform the segmentation, a regional minima is considered to be a connected component of pixels with the same intensity value, whose external boundary pixels all have a higher value. Thus, assigning the value 255 (for 8- bit images) to those pixels in a regional minima and the value 0 to the rest of pixels in I_F , a binary image I_{RM} of relevant regional minima is obtained (Figure 6, images R-2 and G-2):

$$I_{RM}(x, y) = \begin{cases} 255 & if\ (x, y) \in RM \\ 0 & otherwise \end{cases} \tag{2}$$

where *RM* is a regional minima. It is possible that I_{RM} does not contain any segmented connected component. This situation is due to two possible causes. The first cause is that there was not any valley in image *I* with a depth higher or equal to *h* and, therefore, there was not any surviving valley in I_F. The second cause is that, although there were surviving valleys in I_F, they were not regional minima and, therefore, were not segmented. Besides this cause, in the case that I_{RM} does not contain connected components, it is considered that the fovea is not discernible or, at least, not contrasted enough to be segmented safely and the rest of the processing is aborted. On the other hand, I_{RM} can contain more than one segmented connected component if there were more than one regional minima in I_F. In this case, the largest connected component in I_{RM} has the highest probability of being the fovea and therefore is selected as the fovea candidate, resulting from this operation the image I_{FC} (Figure 6, images R-3 and G-3):

$$I_{FC}(x,y) = \begin{cases} 255 & if\ (x,y) \in CC_{MAX} \\ 0 & otherwise \end{cases} \quad (3)$$

where CC_{MAX} is the connected component in I_{RM} with the maximum number of elements.

In summary, if this point is reached, I_{FC} contains a connected component which is considered as a fovea candidate to be validated. This validation is performed in the following section by analysing its size and shape. With respect to this last feature, since the fovea has a circular shape, the circularity of the candidate will be thoroughly analysed. This analysis supposes a problem if it is directly performed on the connected component in I_{FC}, since this component tends to have an irregular contour. To solve this problem, a new connected component composed of the inner points of a polyhedron surrounding the candidate connected component is finally calculated. To obtain this polyhedron, firstly, the centroid of the component is calculated. Then, the hyperplanes supporting the component defined by the normal vectors taken each 5º apart from 0º to 360º are calculated. Finally, inner points of the calculated polyhedron are extracted (Figure 6, images R-4 and G-4). This process is illustrated in Figure 7.

2) Fovea candidate validation and accurate fovea centre location obtaining:

This stage is reached if at least one fovea candidate of the possible two, one from each of the two considered channels, has been produced from the previous stage. The aim here is to analyse the size and circularity of the obtained candidates to validate or discard them. If a candidate is validated, i.e. if it satisfies the size and circularity criteria, an accurate fovea centre location is calculated; otherwise, the fovea is concluded as undetectable (Figure 6, images R-5 and G-5).

The following set of rules precisely describes the fovea candidate validation process:

- If two fovea candidates were obtained: the candidates from the red and green channel are analysed in terms of size and circularity. There are three possible outcomes:
    - The two candidates are validated: a new accurate fovea centre location is calculated as the centroid of the candidate with higher circularity.
    - Only one candidate is validated: a new accurate fovea centre location is calculated as the centroid of the validated candidate.
    - No candidate is validated: the fovea is concluded as undetectable.
- If only one fovea candidate was obtained: the candidate is analysed in terms of size and circularity. If it is validated, a new accurate fovea centre location is calculated as the centroid of the candidate. Otherwise, the fovea is concluded as undetectable.
- If no candidate was obtained: the fovea is concluded as undetectable.

The size and circularity criteria used for validating candidates are described below.

The size evaluation criterion determines a candidate as valid if its maximum radius is between one half and one fourth of the OD diameter. Anatomically, the fovea radius is between one third and one fourth of the OD diameter, however, the applied processing can increase its size and that is why the radius upper limit is increased from one third to one half of the OD diameter. With respect to the circularity evaluation criterion, classic options available in the literature were tested. Nevertheless, a new approach developed for this purpose was the one providing better results. This new approach is based on comparing areas of the candidate object and a circle centered on the centroid of the candidate with a radius equal to the mean radius of the candidate. The quotient

between non-overlapping area of both objects and the area of the candidate object is concretely calculated. If *C* denotes the described circle and *FC* the fovea candidate object, this operation can be mathematically described as:

$$Circ = \frac{\#(C \cup FC) - \#(C \cap FC)}{\#(FC)} \tag{4}$$

where # denotes the cardinal operation, i.e., the area of an object in the image. Once the circularity criterion is defined, a threshold to decide on whether an object is circular enough has to be established. In order to achieve that, 100 object samples were subjectively classified as being circular or not and their circularity values were calculated according to equation (4). Then, these samples were represented in the feature space to be analysed. A circularity value of 0.25 resulted in providing great class separability. Therefore, an object was definitely determined as circular if its circularity value according to equation (4) was lower or equal to 0.25, and not circular otherwise. The process described above to assess the circularity of an object is illustrated in Figure 8.

C. Final decision of the macula centre location and macular grid establishing

The final stage consists of establishing the macular grading grid making use of the obtained fovea centre location. A fovea centre location estimation and an accurate fovea centre location could also have been previously obtained. If an accurate fovea centre location was obtained, this is the finally selected fovea centre location. Otherwise, the finally selected fovea centre location is the firstly obtained estimation.

The grading grid, widely used by ophthalmologists, consists on a coordinate system centered on the fovea centre location. The coordinate system is set up based on the Early Treatment Diabetic Retinopathy Study Report Number 10 [31]. A retinal image is divided into ten subfields as presented in Figure 9. The radii of the three fovea-centered circles from the innermost to the outermost correspond to (1/3) OD, 1 OD, and 2 OD, respectively. The ten subfields are defined as:

1. Central subfield: area within the inner circle.
2. Four inner subfields (superior, nasal, inferior, and temporal): areas between the inner and middle circles.

3. Four outer subfields (superior, nasal, inferior, and temporal): areas between the middle and outer circles.
4. Far temporal subfield: area temporal to the outer circle and between 225º and 135º for the right eyes or between 45º and 315º for the left eyes.

The described system is used by ophthalmologists to assess illness conditions by labeling lesions in each subfield. The illness diagnosis is made by counting detected lesions, taking into account that their relevance varies according to where they are located. This relevance decreases from the most relevant location, the central subfield (threat of central vision loss), to the less relevant location, the far temporal subfield (threat of peripheral vision loss).

Figure 10 shows application examples of the presented methodology for establishing the macular grading grid. The first row shows results obtained on images affected by DR with no risk of ME, the second row shows results on images from patients affected by DR with risk of ME and the last row shows results on healthy images.

VI. EXPERIMENTAL RESULTS

This section presents the results obtained with the presented methodology. In the first subsection, the measures for performance evaluation and comparison are defined. The second subsection presents the results obtained with the proposed approach. Finally, the third subsection compares the obtained results with those presented in other relevant works present in the literature.

A. Performance measures

The literature was revised to check criteria previously used by other authors to determine an appropriate evaluation criterion. Most of the published works have used the Euclidean distance between the obtained fovea centre location and the real fovea centre location as an evaluation measure [9]–[11], [14], [16]. This has been justified by the lack of border definition of the fovea region. Therefore, this distance-based criterion was selected to evaluate the presented work, although some changes were introduced. Most of the publications have established that an obtained fovea centre location is correct if the distance between this one and the real fovea centre location is less

than 1 times the OD radius (1R criterion). This distance is also accepted here but, in order to perform a more precise evaluation, two additional distances were considered. These distances are 0.5 times the OD radius (0.5R criterion) and 0.25 times the OD radius (0.25R criterion). Therefore, these distances are used to create a quality scale for automatically obtained fovea centre locations described as follows:

- Excellent: an obtained fovea centre location is “Excellent” if it satisfies the 0.25R criterion, i.e., if it is at a distance less or equal to 0.25 times the OD radius from the real fovea centre location.
- Good: an obtained fovea centre location is “Good” if it does not satisfy the 0.25R criterion but satisfies the 0.5R criterion. This is, if it is at a distance greater than 0.25 and less or equal to 0.5 times the OD radius from the real fovea centre location.
- Fair: an obtained fovea centre location is “Fair” if it does not satisfy the 0.5R criterion but satisfies the 1R criterion. This is, if it is at a distance greater than 0.5 and less or equal to 1 times the OD radius from the real fovea centre location.
- Poor: an obtained fovea centre location is “Poor” if it does not satisfy any of the previous criteria. This is, if it is at a distance greater than 1 times the OD radius from the real fovea centre location.

Thus, the interval “Excellent - Fair” is equivalent to the 1R criterion and can be used for comparison to other methods. In addition, the study of all categories provides a more precise method evaluation than that provided by the 1R criterion exclusively.

It is important to point out that, since the OD size presents a substantial variation, using the OD radius measured in each image to apply the distance criteria described above can distort results. To minimize this difficulty, the mean OD radius measured in section V-A was used to this effect. By doing this, the OD radius in the described distance criteria goes from being a variable to a constant.

B. Proposed method evaluation

The methodology was tested on the MESSIDOR and DIARETDB database. With regard to the MESSIDOR dataset, it should be pointed out that 38 of the results of the total 1200 images were not rigorously evaluable since the fovea was completely indiscernible, mainly due to very hard lesions. Visual inspection was used to "evaluate" algorithm behaviour in these cases. The algorithm's result in these cases was the fovea centre estimation, discarding the fovea segmentation. This fact shows evidence of the robustness of the methodology. The visual impression of these results was positive but they were not quantifiable. Therefore, final evaluated results are on 1162 images.

Table I shows the results obtained with the presented algorithm for the 1162 rigorously evaluable images in the MESSIDOR database and for the 89 images in DIARETDB. Regarding the results on the MESSIDOR database, the table shows the average percentage of obtained fovea centres according to the quality scale defined in the previous section for each diagnosis case of DR Grade - Risk of ME (cases diagnosed by specialists of the MESSIDOR project; DR condition from 0 to 4 and risk of ME from 0 to 2). The fovea centre location was Excellent in 66.95% of cases, Good in 21.60% of cases, Fair in 8.87% of cases and Poor in the rest of 2.58% of cases. These figures mean that the algorithm appropriately established the macular grading grid in 97.42% of images (quality range Excellent - Fair), which means success in 1132 cases out of the whole set of 1162 images. The success percentage for retinas affected by DR and for healthy retinas was 96.49% and 98.51%, respectively. In terms of images from patients affected by DR, the success rate was 96.17% for images diagnosed with risk of ME and 96.65% for those images with no risk. Consulting these results, there is not any observable pattern associated to illness condition producing remarkable algorithm performance degradation. With regard to results obtained on the DIARETDB database, figures are also presented in terms of the average percentage of obtained fovea centres in each defined quality interval, although it was not possible to detail them in terms of illness condition since this information was not available. Obtained fovea centres were distributed into the following intervals: 42.70% of cases in Excellent category, 30.34% of cases were Good, 22.47% of cases

resulted to be Fair and 4.49% of cases were Poor. These results indicate success in establishing the macular grading grid in 95.51% of cases, i.e., the process was successful in 85 out of the 89 images.

The presented algorithm was experimentally implemented in Matlab. Tests of computational efficiency of this implementation were performed using a PC equipped with an Intel Core2Duo CPU at 2.13 GHz and 2 GB of RAM capacity. For 1162 executions of the algorithm, the measured average computational time was 10.88 sec. with a standard deviation of 0.19 sec. It should be stressed that a future enhanced implementation using a more proper programming language such as C++ will drastically decrease these figures.

C. Comparison to other methods

Results of the presented methodology are compared to those of other relevant published works in this section from two differing points of view. On the one hand, results obtained on the MESSIDOR dataset are compared to the following methods: Fleming et al. [11], those of Niemeijer et al. [9], [14] and Tobin et al. [10]. It has to be pointed out that these methodologies were tested on local and not public databases. This means that it makes it impossible to perform a comparison under identical conditions. In spite of this, the image description provided by their corresponding authors (images from screening programs of DR) indicates that the nature of the used datasets for testing is similar to the nature of the images in the MESSIDOR database. Therefore, this author considers that information provided by this comparison may be of interest to get a good idea about the behaviour and competitiveness of the presented work. On the other hand, results obtained on the DIARETDB database are compared to the following set of works: Welfer et al. [16], Sinthanayothin et al.[15], Narasimha-Iyer et al. [17], Singh et al. [18], Sagar et al. [19], Sopharak et al. [20] and Sekhar et al. [21]. Results of all these methodologies on the DIARETDB are available at Welfer et al. [16], so a more rigorous comparison is possible to be performed in this case.

Fleming et al. [11] evaluated their results according to the 1R criterion. Niemeijer et al. [9], [14] used in their works a distance in number of pixels to decide on when an obtained fovea centre was correct. In spite of this, the distance used by those authors, according to the image resolution and FOV size used by them, is approximately equal to the distance established by the 1R criterion. The

same situation occurs with the works by Welfer et al. [16], Sinthanayothin et al.[15], Narasimha-Iyer et al. [17], Singh et al. [18], Sagar et al. [19], Sopharak et al. [20] and Sekhar et al. [21]. The defined distance for testing is equivalent to the 1R criterion. Therefore, the results of these works are comparable with those of the presented methodology using this distance. On the other hand, Tobin et al. [10] considered an obtained fovea centre as valid if it was located at a distance less or equal to 2 times the OD radius from the true fovea centre (2R criterion). Therefore, the work described here was also evaluated using the 2R criterion with the aim of comparing both approaches.

Table II and III show the results of the above mentioned methodologies compared to the one presented in this paper (referred to as Morphological Method) on the MESSIDOR and DIARETDB database, respectively. As it can be observed, results obtained with the presented methodology on both datasets can at least be measured up to the best analysed works.

VII. DISCUSSION AND CONCLUSION

Two types of criteria have been historically used for segmenting the fovea: anatomical and visual feature-based criteria. The methodology presented in this chapter takes advantage of both approaches. It is divided into three main stages: (A) obtaining a fovea centre estimation by using anatomical feature-based criteria, (B) obtaining an accurate fovea centre location if this is detectable by using visual feature-based criteria, and (C) final fovea centre decision and macular grading grid establishing.

The main contribution of the presented work is the processing applied in stage (B). To the best of the author's knowledge, published methodologies based on visual features of the fovea perform a rigid processing in which the fovea is assumed to always be present. On the contrary, the morphological processing applied in this work discards the accurate location of the fovea if no valid candidates were found. The fovea centre estimation obtained in stage (A) is used to identify the macular zone in this case. This approach makes the process more safe and stable.

To test the proposed methodology, a quality scale based on the distance of the obtained fovea centre to the true fovea centre was defined. This scale contains four categories: Excellent, Good, Fair and Poor. Table I summarizes the obtained results according to this quality scale. The methodology

obtained valid fovea centres, those in the range Excellent - Fair, in 97.42% of the 1162 rigorously evaluable images in the MESSIDOR database and 95.51% of the 89 images in the DIARETDB dataset. Furthermore, the methodology obtained fovea centres in the range Excellent - Good in 88.5% and 73.01% of cases in the MESSIDOR and DIARETDB dataset, respectively. The reason why this outstanding algorithm's behaviour is slightly worse in the case of the DIARETDB database may be understood by studying the nature of the images. This dataset was collected to include lesions mainly near the macula and great image variability in terms of noise, illumination and other technical aspects. These issues seem to moderately affect the finer accuracy. On the other hand, Table II and III show the competitiveness of obtained results when comparing them to other relevant published methods. The algorithm computational efficiency should also be mentioned since it is also related to testing. Tests made on a mid-range PC gave a mean computational time of 10:88 sec. with a standard deviation of 0:19 sec. Although these figures are already acceptable, since the method implementation is experimental they can easily be improved.

In the context of computer-aided detection of DR and other retinal pathologies, robust macular zone identification by means of grading grid establishing is of vital importance since relevance of lesions is related to their location regarding the macula. In this respect, since the presented methodology is fully automatic, it may be useful in a great amount of environments. Not in vain, the final objective is to put at the disposal of the scientific community a professional screening software including this work. For instance, it could help by decreasing workload in the context of preventive screening programs or in the context of specialist illness condition assessing. On the other hand, since this methodology segments the fovea only when this is visible and, in the other case provides an estimation of its location, it could also be helpful in surgical environments for treatment of, for instance, maculopathy. In essence, the software could provide the ophthalmologists the macular grading grid for laser application guidance. Furthermore, the software could even allow the grid interactive movement in the case the specialist would like to modify its position. The reliability, robustness and efficiency obtained with the methodology presented in this paper, show evidence that its integration in those kinds of situations may be successful.

ACKNOWLEDGMENT

The author would like to thank the MESSIDOR and DIARETDB program partners for facilitating their database.

REFERENCES

[1] H. Taylor, J. Keeffe, Costs of mobile screening for diabetic retinopathy: A practical framework for rural populations, Br. J. Ophthalmol. 85 (2001) 261-266.

[2] S. Wild, G. Roglic, A. Green, R. Sicree, H. King, Global prevalence of diabetes: estimates for the year 2000 and projections for 2030, Diabetes Care 27 (2004) 1047-1053.

[3] S. Lee, C. McCarty, H. Taylor, J. Keeffe, World blindness: a 21st century perspective, Aust. J. Rural Health 8 (2001) 186-192.

[4] G. Bresnick, D. Mukamel, J. Dickinson, D. Cole, A screening approach to the surveillance of patients with diabetes for the presence of vision-threatening retinopathy, Opthalmology 107 (2000) 19-24.

[5] Early Treatment Diabetic Retinopathy Study Research Group, Early photocoagulation for diabetic retinopathy: Etdrs report 9, Opthalmology 98 (1991) 766-785.

[6] D. Fong, L. Aiello, T. Gardner, G. King, G. Blankenship, J. Cavallerano, F. Ferris, R. Klein, Diabetic retinopathy, Diabetes Care 26 (2003) 226-229.

[7] H. Larsen, The Ocular Fundus: A Color Atlas, Copenhagen, Denmark: Munksgaard, 1976.

[8] J. Schwiegerling, Field Guide to Visual and Ophthalmic Optics, Bellingham, WA: SPIE., 2004.

[9] M. Niemeijer, M.D. Abràmoff, B. van Ginneken, Segmentation of the optic disc, macula and vascular arch in fundus photographs, IEEE Transactions on Medical Imaging 26 (2007) 116-127.

[10] K. Tobin, E. Chaum, V. Govindasamy, T. Karnowski, Detection of anatomic structures in human retinal imagery, IEEE Trans. Med. Imag. 26 (2007) 1729-1739.

[11] A. Fleming, K. Goatman, S. Philip, J. Olson, P. Sharp, Automatic detection of retinal anatomy to assist diabetic retinopathy screening, Phys. Med. Biol. 52 (2007) 331-345.

[12] L. Gagnon, M. Lalonde., M. Beaulieu, M.-C. Boucher, Procedure to detect anatomical structures in optical fundus images, in: Proc. SPIE Med. Imaging: Image Processing, 2001, vol. 4322, 2001, pp. 1218-1225.

[13] H. Li, O. Chutatape, Automated feature extraction in color retinal images by a model based approach, IEEE Trans. Biomed. Eng. 51 (2004) 246-254.

[14] M. Niemeijer, M.D. Abràmoff, B. van Ginneken, Fast detection of the optic disc and fovea in color fundus photographs, Medical Image Analysis 13 (2009) 859-870.

[15] C. Sinthanayothin, J. Boyce, H. Cook, T. Williamson, Automated localisation of the optic disc, fovea, and retinal blood vessels from digital colour fundus images, Br. J. Ophthalmol. 83 (1999) 902-910.

[16] D. Welfer, J. Scharcanski, D.R. Marinho, Fovea center detection based on the retina anatomy and mathematical morphology.

[17] H. Narasimha-Iyer, A. Can, B. Roysam, C.V. Stewart, H.L. Tanenbaum, A. Majerovics, H. Singh, Robust detection and classification of longitudinal changes in color retinal fundus images for monitoring diabetic retinopathy, IEEE Transactions on Biomedical Engineering 53 (6) (2006) 1084‑1098.

[18] J. Singh, G.D. Joshi, J. Sivaswamy, Appearance based object detection in colour retinal images, in: IEEE International Conference on Image Processing, IEEE, San Diego, CA, USA, 2008.

[19] A.V. Sagar, S. Balasubramanian, V. Chandrasekaran, Automatic detection of anatomical structures in digital fundus retinal images, in: IAPR Conference on Machine Vision Applications, Tokyo, Japan, 2007, pp. 483‑486.

[20] A. Sopharak, B. Uyyanonvara, S. Barmanb, T.H. Williamson, Automatic detection of diabetic retinopathy exudates from non-dilated retinal images using mathematical morphology methods, Computerized Medical Imaging and Graphics 32 (2008) 720‑727.

[21] S. Sekhar, W. Al-Nuaimy, A. Nandi, Automated localization of optic disk and fovea in retinal fundus images, in: 16th European Signal Processing Conference (EUSIPCO-2008), Lausanne, Switzerland, 2008.

[22] Download images section, MESSIDOR: Digital Retinal Images, MESSIDOR TECHNO-VISION Project, France [Online]:http://messidor.crihan.fr/download-en.php

[23] T. Kauppi, V. Kalesnykiene, J.-K. Kamarainen, L. Lensu, I. Sorri, A. Raninen, R. Voutilainen, H. Uusitalo, H. Kalviainen, J. Pietila, DIARETDB1 diabetic retinopathy database and evaluation protocol, in: Medical Image Understanding and Analysis (MIUA), 2007, pp. 61‑65.

[24] A. Aquino, M.E. Gegúndez-Arias, D. Marín, Detecting the Optic Disc Boundary in Digital Fundus Images Using Morphological, Edge Detection, and Feature Extraction Techniques, IEEE Trans. Med. Imag. 29 (2010) 1860-1869.

[25] D. Marin, A. Aquino, M.E. Gegúndez-Arias, J.M. Bravo, A New Supervised Method for Blood Vessel Segmentation in Retinal Images by Using Gray-Level and Moment Invariants-Based Features, IEEE Trans. Med. Imag. 30 (2011) 146-158.

[26] J. Serra, Image Analysis and Mathematical Morphology Vol. 1, Academic Press, London, 1982.

[27] H. Li, O. Chutatape, Automatic location of optic disc in retinal images, in: Proc. IEEE Int. Conf. on Image Proc., 2001, pp. 837-840.

[28] Results section-sample databases, Expert System for Early Automated Detection of Diabetic Retinopathy by Analysis of Digital Retinal Images Project, Spain [Online]:http://www.uhu.es/retinopathy/eng/index.php

[29] T. Walter, J. Klein, Handbook of Biomedical Image Analysis. Vol. 2 - Ch. Automatic analysis of color fundus photographs and its application to the diagnosis of diabetic retinopathy, Kluwer Academic/Plenum, pp. 315-368, 2005.

[30] P. Soille, Morphological Image Analysis: Principles and Applications, Springer-Verlag, Germany: Berlin, 1999.

[31] Early Treatment Diabetic Retinopathy Study Research Group, Grading diabetic retinopathy from stereoscopic color fundus photographs-an extension of the modified airlie house classification. ETDRS report number 10, Ophthalmology 98 (1991) 786-806.

FIGURES

Fig. 1. Fovea appearance in eye fundus images: (a) The fovea is easily recognizable as a round dark area. (b) The fovea is not visible due to the presence of lesions.

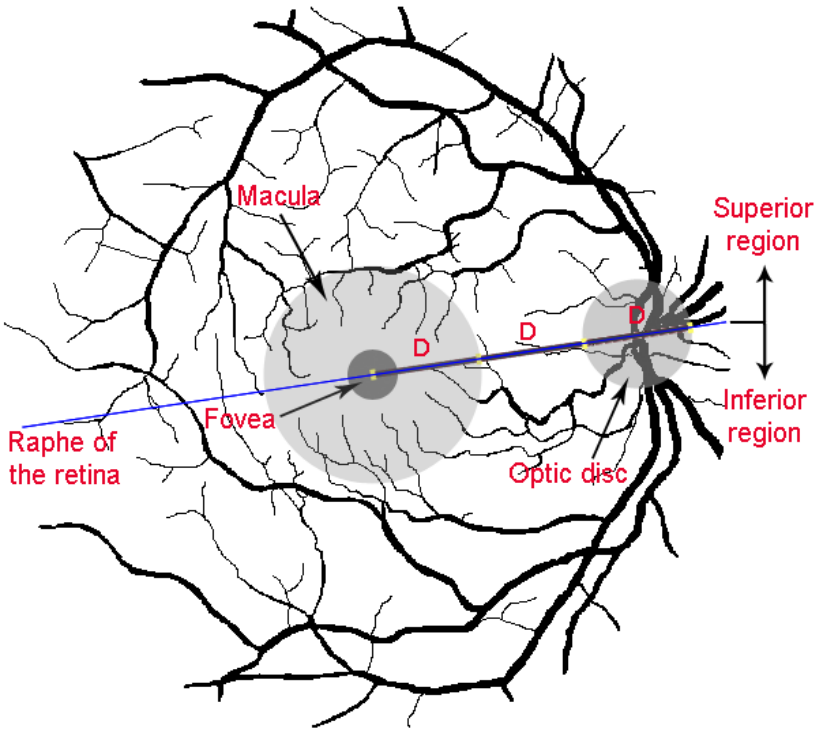

Fig. 2. Diagram illustrating macula features in the eye fundus.

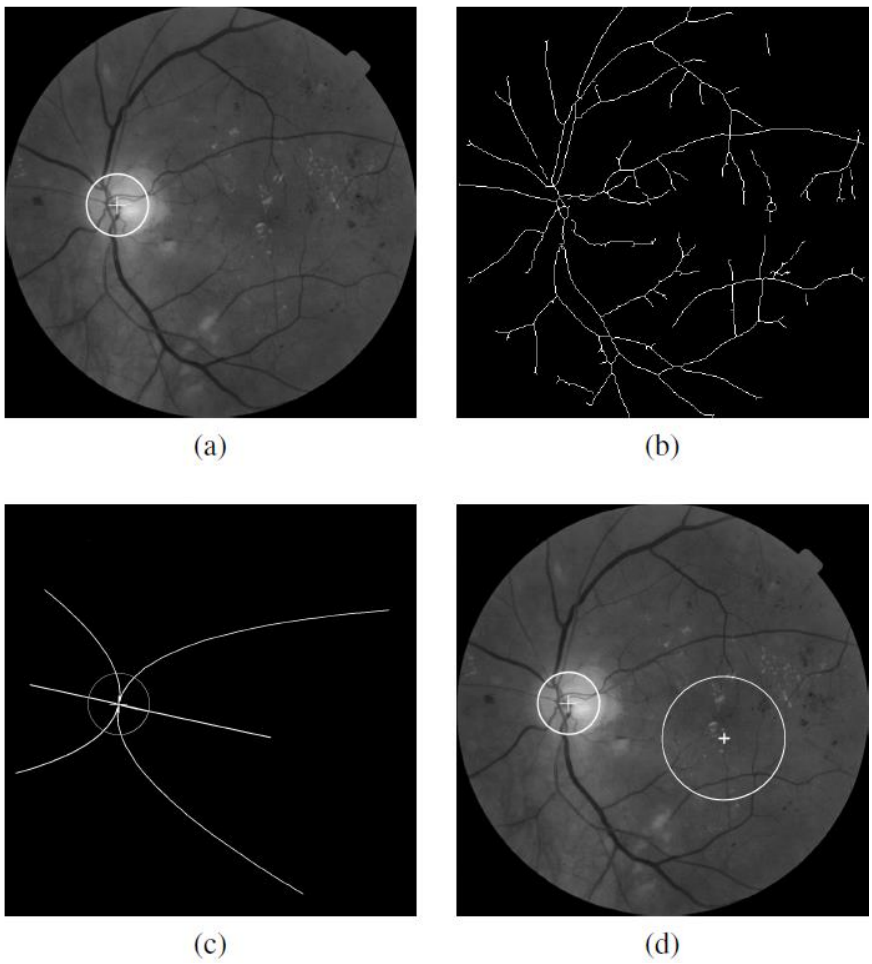

Fig. 3. (a) Optic disc (OD) segmentation with centre in (x_{OD}, y_{OD}) = (375, 665) and diameter D_{OD} = 210 pixels. (b) Skeletonized segmentation of the vascular tree $b_t\ (x, y)$. (c) Parabolic model centered on (X_{OD}, y_{OD}) and applied to $b_t\ (x, y)$. (d) fovea centre estimation. The fovea centre is estimated by using the known OD centre in (a), applying a geometric model to the skeletonized segmented vascular tree in (b) to determine the approximate horizontal raphe in (c), and positioning the fovea centre along the raphe accordingly in (d).

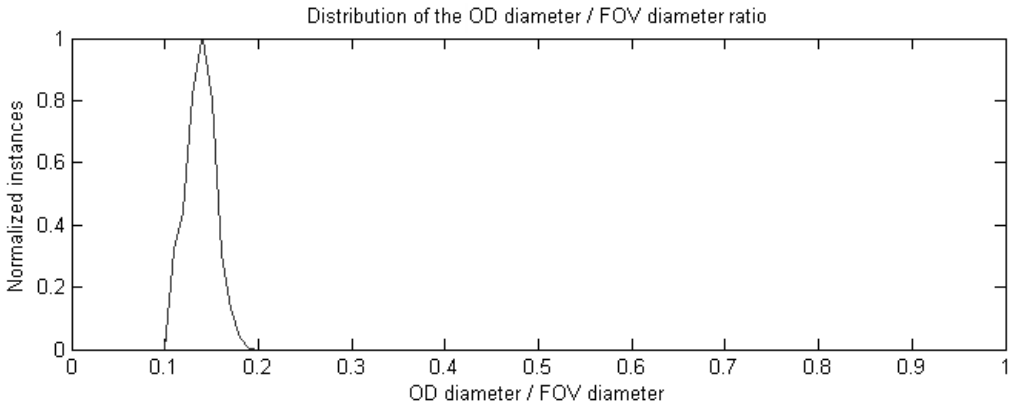

Fig. 4. Distribution of the relative optic disc (OD) size in eye fundus images. This relative OD size is measured as the ratio between the maximum OD diameter and the diameter of its corresponding field-of-view; data is shown normalized to the interval [0, 1]. As it can be observed, the relative OD size follows a Gaussian distribution, whose average and standard deviation are 0.1382 and 0.0149, respectively.

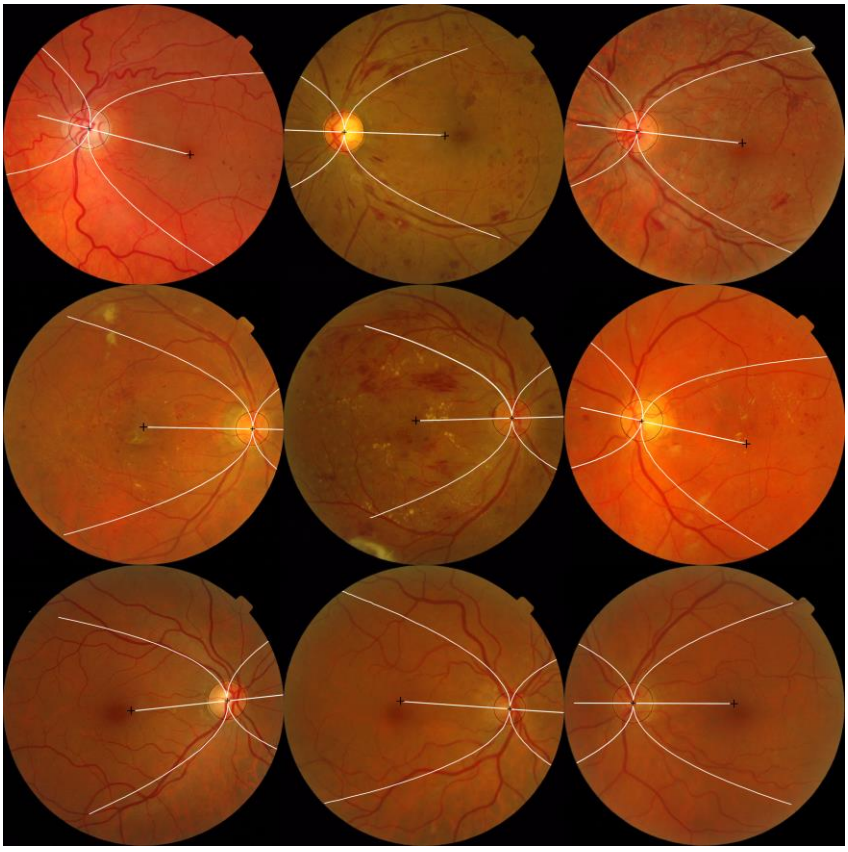

Fig. 5. Examples of the fovea centre estimation. The first row shows three retinographies from patients with diabetic retinopathy and with no risk of macular edema, the second is composed of

three retinographies from patients affected by diabetic retinopathy and with risk of macular edema and the last three images are from healthy retinas.

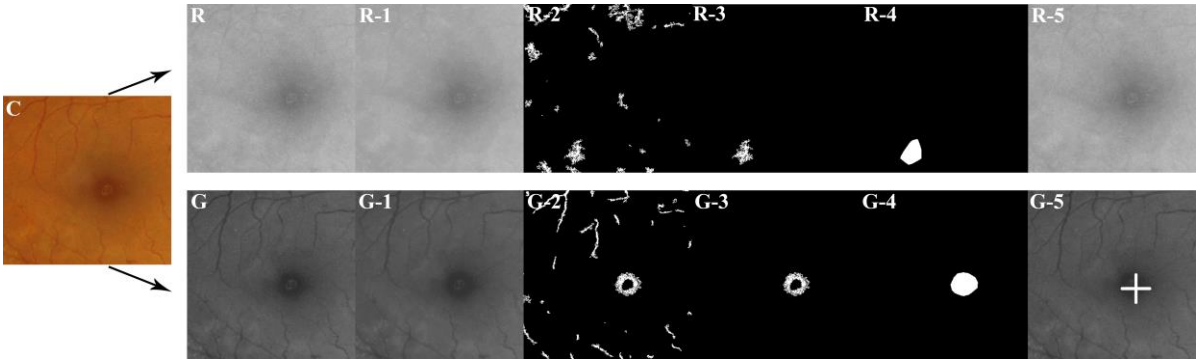

Fig. 6. Illustration of the process for accurate fovea centre location: (C) Initial RBG fovea-containing subimage. On the right, the top row shows the process performed on the red channel, whereas the bottom corresponds to the process applied to the green component. (R) and (G) Sub-images extracted from the red and green channels of (C), respectively. (R-1) and (G-1) Result of the H-minima transform. (R-2) and (G-2) Regional minima image. (R-3) and (G-3) Image containing the fovea candidate. (R-4) and (G-4) Convex hull of the fovea candidate. (R-5) and (G-5) accurate fovea centre location. The candidate in image (R-5) is discarded since it has a circularity value of 0.3695. The candidate in (G-5) has a correct size and a circularity value of 0.0969, therefore it is validated and the accurate fovea centre location is the location of its centroid.

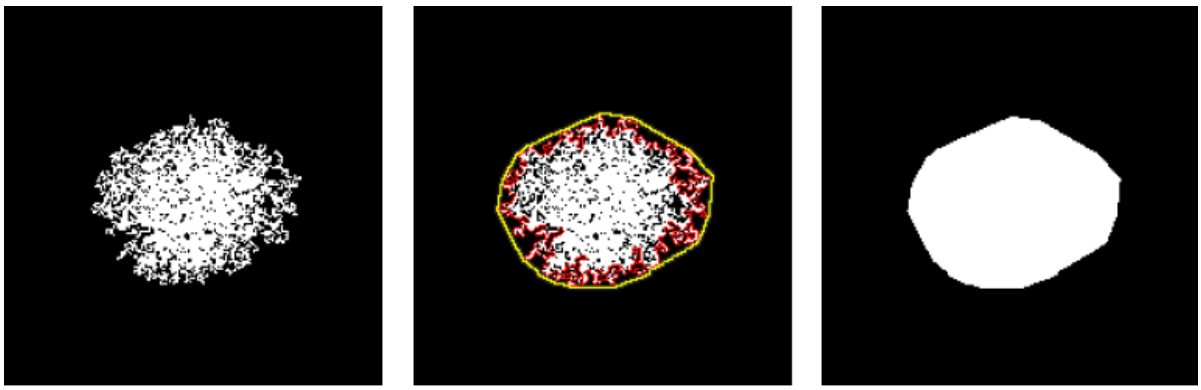

Fig. 7. Illustration of the process for obtaining the surrounding polyhedron of a segmented object: (a) Segmented object. (b) The boundary of (a) is marked in red colour and the convex hull of that boundary is traced in yellow colour. The convex hull is obtained by linearly interpolating points of

the object contour taken each 5 degrees apart from 0 to 360 degrees. (c) The obtained surrounding polyhedron.

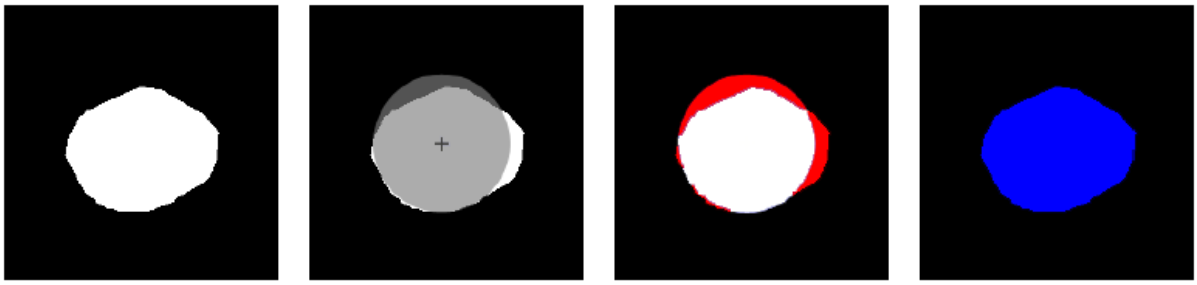

Fig. 8. Process to assess the circularity of an object: (a) Object to be analysed. (b) Circle centered on the centroid of (a) with radius equal to the mean radius of (a). (c) The non-overlapping area between (a) and the circle in (b) is represented in red colour. (d) The area of (a) is represented in blue colour. The circularity of (a) is calculated as the quotient of the red area in (c) and the blue area in (d). In this case, (a) is validated as circular, since its circularity value is 0.1149.

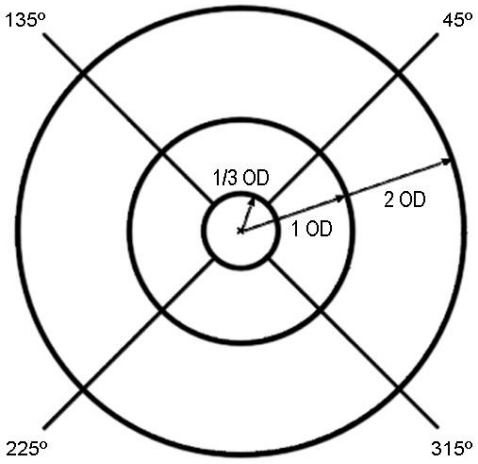

Fig. 9. Polar coordinate system centered on the fovea.

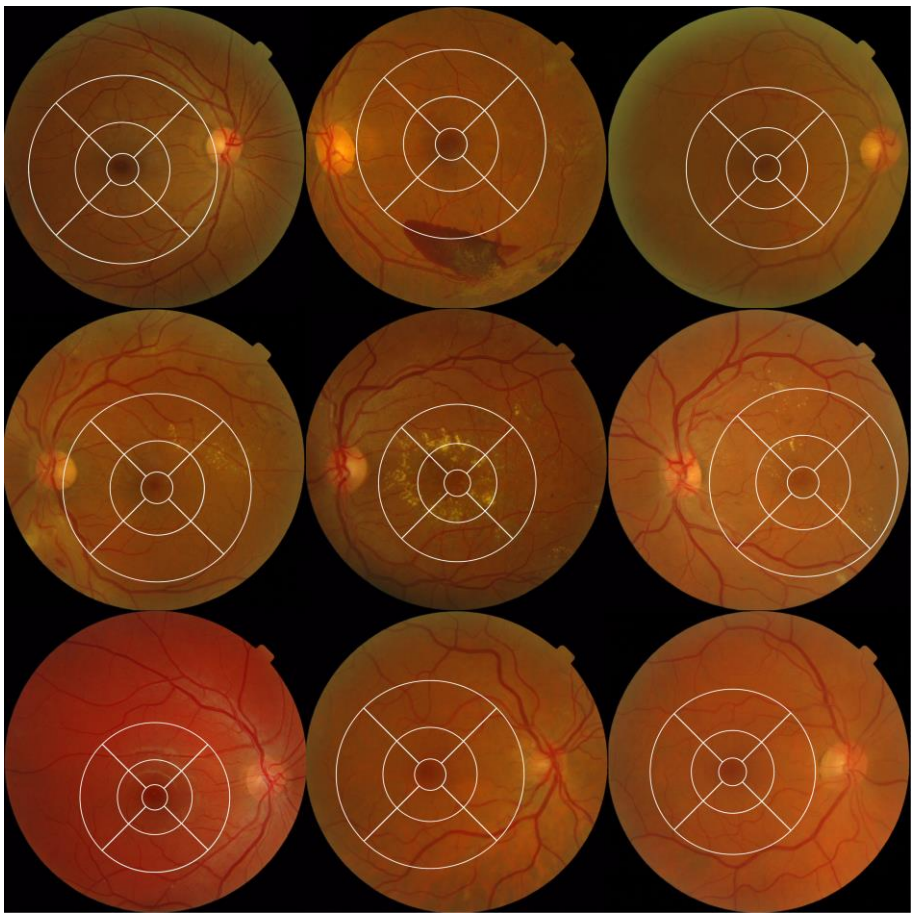

Fig. 10. Examples of the macular grading grid establishing. The first row shows three retinographies from patients with diabetic retinopathy and with no risk of macular edema, the second is composed of three retinographies from patients affected by diabetic retinopathy and with risk of macular edema and the last three images are from healthy retinas.

TABLES

MESSIDOR						
DR Grade – Risk of ME	**Cases**	**Excellent**	**Good**	**Fair**	**Poor**	**Excellent – Fair**
0-0	535	71.78%	20.37%	6.36%	1.49%	98.51%
1-0	142	76.76%	17.60%	3.53%	2.11%	97.89%
1-1	5	80.0%	20.0%	0.0%	0.0%	100.0%
1-2	6	100.0%	0.0%	0.0%	0.0%	100.0%
2-0	179	67.04%	22.91%	7.82%	2.23%	97.77%
2-1	28	71.43%	17.86%	7.14%	3.57%	96.43%
2-2	37	51.35%	29.73%	18.92%	0.0%	100.0%
3-0	97	45.36%	28.86%	18.56%	7.22%	92.78%
3-1	41	65.85%	24.39%	9.76%	0.0%	100.0%
3-2	92	48.91%	22.83%	20.65%	7.61%	92.39%
Total	**1162**	**66.95%**	**21.60%**	**8.87%**	**2.58%**	**97.42%**
DIARETDB						
	Cases	**Excellent**	**Good**	**Fair**	**Poor**	**Excellent – Fair**
	89	**42.70%**	**30.34%**	**22.47%**	**4.49%**	**95.51%**

Table I: results of the algorithm for macular zone identification according to the defined quality scale. Results are given for the MESSIDOR and DIARETDB as the average percentage of obtained fovea centre locations in each quality category. Additionally, results on the MESSIDOR database are detailed per diagnosis case since this information is provided by the database partners.

Method	Images	1R criterion	2R criterion
Fleming *et al.* [11]	1056	95.50%	-
Niemeijer *et al.* [9]	500	94.40%	-
Niemeijer *et al.* [14]	500	96.80%	-
Tobin *et al.* [10]	345	-	92.50%
Morphological Method (this work)	**1162**	**97.42%**	**98.36%**

Table II: results of the presented algorithm for macular zone identification on the MESSIDOR database compared to other approaches present in the literature. Results of methods from other authors were obtained on private databases collected from retinal screening programs.

Method	Images	1R criterion
Sinthanayothin *et al.*[15]	89	65.16%
Narasimha-Iyer et al. [17]	89	80.89%
Singh *et al.* [18]	89	65.16%
Sagar *et al.* [19]	89	84.26%
Sopharak *et al.* [20]	89	38.20%
Sekhar *et al.* [21]	89	67.41%
Welfer *et al.* [16]	89	92.13%
Morphological Method (this work)	**89**	**95.51%**

Table III: results of the presented algorithm for macular zone identification on the DIARETDB database compared to other present in the literature. Results of compared methods were produced by implementations made by Welfer et al [16].